Radardetected englacial debris in the West Antarctic Ice Sheet

Geophysical Research Letters

RESEARCH LETTER
10.1029/2019GL084012

Radar-Detected Englacial Debris in the West Antarctic Ice Sheet

Kate Winter[1], John Woodward[1], Neil Ross[2], Stuart A. Dunning[2], Andrew S. Hein[3], Matthew J. Westoby[1], Riley Culberg[4], Shasta M. Marrero[3], Dustin M. Schroeder[4,5], David E. Sugden[3], and Martin J. Siegert[6]

[1]Department of Geography and Environmental Sciences, Faculty of Engineering and Environment, Northumbria University, Newcastle upon Tyne, UK, [2]School of Geography, Politics and Sociology, Newcastle University, Newcastle upon Tyne, UK, [3]School of Geosciences, University of Edinburgh, Edinburgh, UK, [4]Department of Electrical Engineering, Stanford University, Stanford, CA, USA, [5]Department of Geophysics, Stanford University, Stanford, CA, USA, [6]Grantham Institute and Department of Earth Science and Engineering, Imperial College London, London, UK

Key Points:
- Ice-penetrating radar reveals basal sediment reflectors in the West Antarctic Ice Sheet
- Basal thermal regimes promote sediment entrainment
- Once entrained, basal sediments are transported by regional ice flow

Supporting Information:
- Supporting Information S1

Correspondence to:
K. Winter,
k.winter@northumbria.ac.uk

Citation:
Winter, K., Woodward, J., Ross, N., Dunning, S. A., Hein, A. S., Westoby, M. J., et al. (2019). Radar-detected englacial debris in the West Antarctic Ice Sheet. *Geophysical Research Letters*, *46*. https://doi.org/10.1029/2019GL084012

Received 5 JUN 2019
Accepted 21 AUG 2019
Accepted article online 26 AUG 2019

Abstract Structural glaci-geological processes can entrain basal sediment into ice, leading to its transportation and deposition downstream. Sediments potentially rich in essential nutrients, like silica and iron, can thus be transferred from continental sources to the ocean, where deposition could enhance marine primary productivity. However, a lack of data has limited our knowledge of sediment entrainment, transfer, and distribution in Antarctica, until now. We use ice-penetrating radar to examine englacial sediments in the Weddell Sea sector of the West Antarctic Ice Sheet. Radargrams reveal englacial reflectors on the leeside of nunataks and subglacial highlands, where Mie scattering analysis of the reflectors suggests particle sizes consistent with surface moraine sediments. We hypothesize that these sediments are entrained at the thermal boundary between cold and warm-based ice. Conservative estimates of $>130 \times 10^9$ kg of englacial sediment in Horseshoe Valley alone suggest that the ice sheet has significant entrainment potential unappreciated previously.

Plain Language Summary Glaciers can acquire and transport sediments rich in essential nutrients, like silica and iron, from the land to the ocean, where deposition may enhance biological productivity. Our ability to detect and map sediment-rich ice in Antarctica has been hindered by technical limitations of geophysical equipment and data availability, until now. In this paper ice-penetrating radar is used to detect sediments in the Weddell Sea sector of the West Antarctic Ice Sheet. We identify sediment near the glacial surface, and further down the ice column, along partially buried mountain ranges and bedrock hills beneath the ice. Our conservative estimates reveal >130 million metric tonnes of englacial sediment in a single valley. These sediments are entrained at the ice/bed interface and transported to mountain fronts and the coast by local and regional ice flow.

1. Introduction

Once entrained in glacier ice, sediments, including those rich in essential nutrients like silica and iron, can be transferred from continental sources to the ocean by ice flow, and then iceberg production and transport (Death et al., 2014; Hawkings et al., 2014, 2018; Nicholls et al., 2012). This can create layers of ice-rafted debris in deep-sea deposits (Leventer et al., 2006; Pierce et al., 2011), such as the North Atlantic Heinrich layers (Heinrich, 1998). In Antarctica, these offshore deposits are used to reconstruct inland sediment sources, and assess past changes in the locus of glacial erosion (Licht & Hemming, 2017; Wilson et al., 2018). Offshore sediments have also been used to examine glacially derived bioavailable iron concentrations (Shoenfelt et al., 2018), which can impact primary productivity and CO_2 drawdown in the Southern Ocean (Death et al., 2014; Hawkings et al., 2014, 2018). While the significance of sediment entrainment, transfer, and deposition are understood, observations of englacial sediment in large ice sheets, which can corroborate interpretations of marine sedimentary records, are rare. This is a function of both ice-penetrating radar (IPR) resolution and data availability. Recent improvements in the collection and processing of IPR data allow us to investigate mechanisms of sediment entrainment and transfer in the Weddell Sea sector of the West Antarctic Ice Sheet (WAIS).

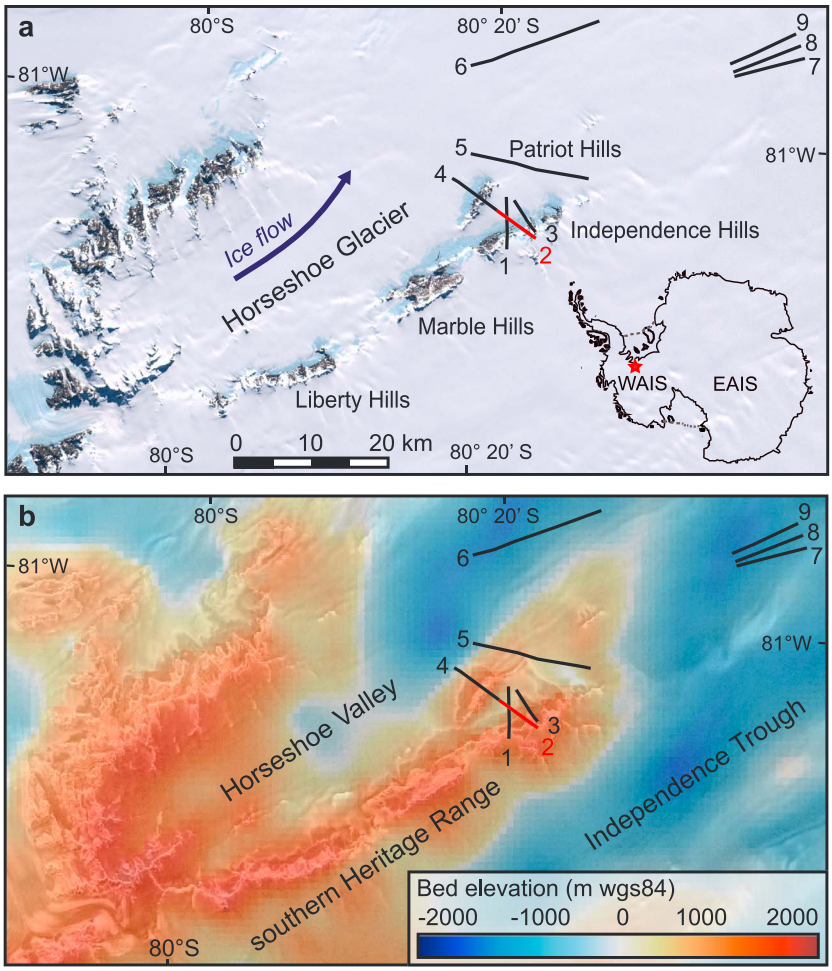

Figure 1. Horseshoe Valley, West Antarctica. (a) Landsat Image Mosaic of Antarctica (LIMA) (USGS: http://lima.usgs.gov/) contextualizing the Patriot and Independence Hills in Horseshoe Valley (marked on the inset map of Antarctica) and the location of airborne radio echo sounding (RES) transects 1–9. Note that airborne RES transect 2 is marked in red, to differentiate its reduced length in Figure 2d from the whole flight line (transect 4) used in Figure 3a. (b) Bed elevation plot (Fretwell et al., 2013) superimposed over RADARSAT (Liu et al., 2001) to show the relief of Horseshoe Valley, its delimiting mountains, and the neighboring Independence Trough.

2. Study Area

We analyze englacial reflectors, recorded by both regional airborne radio echo sounding (RES) and local ground-based IPR, in and around Horseshoe Valley (80°018′S, 81°122′W), which is in the southern Heritage Range of West Antarctica (Figure 1). These mountains separate the ~20-km-wide and >2,000-m-thick Horseshoe Glacier (Winter et al., 2015), which flows at 8–12 m/a (Rignot et al., 2017), from neighboring ice flow, and channelize ice in Horseshoe Valley toward the Filchner-Ronne Ice Shelf, ~45 km away at Hercules Inlet. Sharp peaks, ridges, and bedrock spurs constrain topographic embayments on the leeward slopes of the Liberty, Marble, Independence, and Patriot Hills of Horseshoe Valley (Figure 1) where enhanced sublimation by katabatic winds cause ice and basal debris to flow toward the mountain front, forming extensive blue ice areas and associated blue ice moraines (Fogwill et al., 2012; Hein et al., 2016; Sugden et al., 2017; Figure 2). These glacial and atmospheric processes cause previously horizontal englacial layers to flow up toward the mountain front (Winter et al., 2016), exhuming glacially entrained sediment clasts that often exhibit glacial abrasion, in the form of subangular to subrounded shapes and millimeter-scale striations (Figures 2b and 2c) and exposing inclined isochrone sequences at the glacial surface (Turney et al., 2013). The existence of subglacially transported clasts and exotic lithologies in Horseshoe Valley blue ice moraines and historical interpretation of moraine sediment in local IPR transects (Doake,

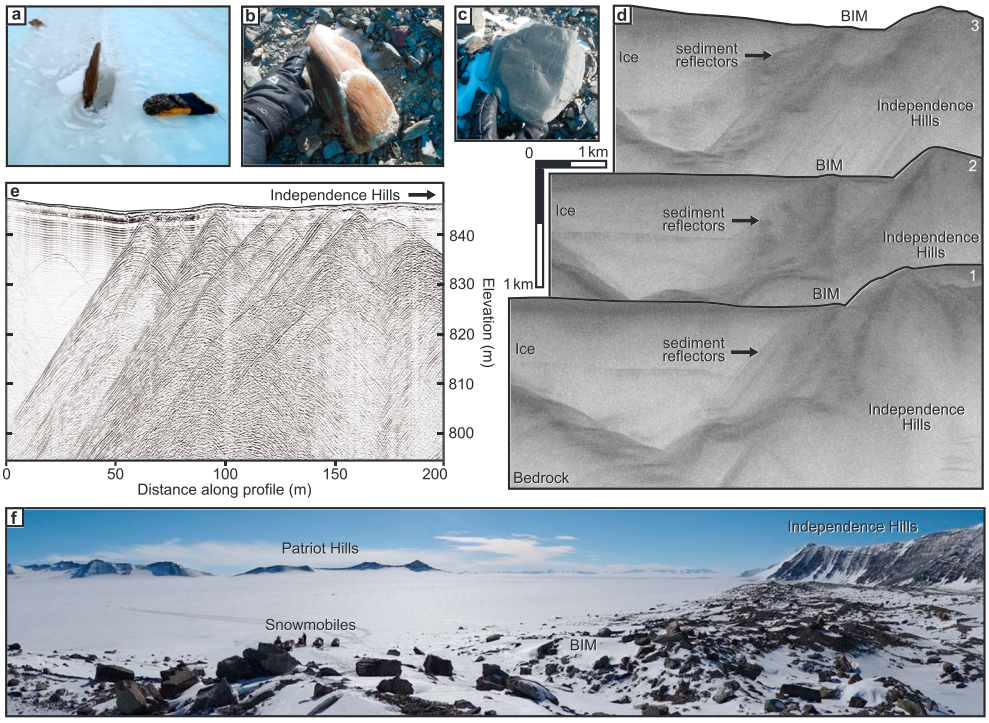

Figure 2. Characterization of Independence Hills Blue Ice Moraine. (a) Sediment emerging from blue ice in Horseshoe Valley. (b) Sediment clast with subrounded shape and straight, parallel striations. (c) Sediment clast with subangular shape and multiple striations, in a variety of orientations. (d) Airborne RES transects across a valley glacier and Independence Hills (shown in photograph f) reveal englacial reflectors which extend from the ice/bed interface to Blue Ice Moraine (BIM) deposits in the lee of Independence Hills. (e) Hyperbolic reflectors in an IPR transect (collected across the BIM sequence at the base of Independence Hills) reveal seven linear features beneath the sediment-strewn surface (shown in photograph f).

1981) make Horseshoe Valley well suited for investigation of basal sediment entrainment and transfer processes in Antarctica.

3. Methods

3.1. Ground Based Ice-Penetrating Radar

A sledge-mounted PulseEkko 1000 system, operating at 200 MHz, was used to acquire high-resolution IPR data from Horseshoe Valley at 0.1-m intervals in the austral summer of 2012/2013 (Winter et al., 2016). IPR survey antenna were co-polarized and orientated perpendicular to the survey lines, with their broadsides parallel to each other. Differential GPS was collected to enable topographic correction to decimeter accuracy. ReflexW (2012) radar processing software (version 6.1.1; Sandmeier Scientific Software, 2012) was used to process IPR data using standard processing steps (King, 2011; Welch & Jacobel, 2005; Woodward & King, 2009), including time zero correction, band-pass filtering, and application of an energy decay gain. As point reflectors are more apparent in unmigrated data, migration was not applied. To convert travel time to ice thickness a standard electromagnetic wave propagation speed in ice of 0.168 m/ns was applied.

3.2. Airborne Radio Echo Sounding

The British Antarctic Survey Polarimetric-radar Airborne Science Instrument ice-sounding radar system (Jeofry et al., 2018) was used to collect RES data in and around Horseshoe Valley in the austral summer of 2010/2011 for the British Antarctic Survey Institute Möller Antarctic Funding Initiative survey (https://doi:10.5285/8a975b9e-f18c-4c51-9bdb-b00b82da52b8). PASIN operates at a frequency of 150 MHz, using a pulse-coded waveform acquisition rate of 312.5 Hz and bandwidth of 12 MHz. Aircraft position was obtained from differential GPS, while terrain clearance was measured using radar/laser altimeters. Removal of radar-scattering hyperbolae in the along-track direction was achieved through two-dimensional focused Doppler

(synthetic aperture radar) processing. This technique also enhanced basal features. As a function of this processing, the uppermost 200 samples (~150–200 m) of synthetic aperture radar-processed radargrams are often poorly resolved, so non two-dimensional SAR pulse data were used to investigate near-surface reflections (RES lines 1–3; Figure 2d). An electromagnetic wave propagation speed of 0.168 m/ns and a 10-m firn correction was applied to all RES transects (Ross et al., 2012). Technical details of the Polarimetric-radar Airborne Science Instrument system and additional details on the acquisition and processing of the Institute Möller Antarctic Funding Initiative RES data are available in Jeofry et al. (2018), and references therein.

3.3. Mie Scattering Analysis

To assess the likelihood that englacial reflectors in RES data are entrained sediments, we apply Mie theory (Aglyamov et al., 2017) to quantify the sediment grain sizes required to produce the observed echo powers and compare these estimates to surface sediment grain sizes from Patriot Hills, recorded by Westoby et al. (2015). Under this model, entrained sediment is treated as a random collection of spherical particles of some mean radius occupying some fraction of the ice volume. The total power received by the radar is then the sum of the power backscattered by every particle in the illuminated volume (Ulaby & Long, 2014). Knowing the echo power, radar system parameters, and flight geometry, we set the fractional volume and solve the volumetric radar equation (Ulaby & Long, 2014) for the Mie backscatter coefficient, a function of particle size and material. An open-source Mie solver (Mätzler, 2002) was used to invert for the estimated particle radius. Further details of these methods, particularly the radiometric calibration of the radargrams and associated uncertainties, are described in the supporting information.

4. Results

Our geophysical observations reveal steeply dipping englacial reflectors, extending from the ice/bed interface up to blue ice moraine complexes in the foreground of exposed bedrock along the margins of the southern Heritage Range (Figure 2). Similar reflectors are recorded in Horseshoe Valley Glacier beneath >1.4 km of ice (Figure 3). These reflectors are explored in the following paragraphs.

4.1. Englacial Reflectors

In the lee of Independence Hills, englacial reflectors are recorded in several airborne RES transects, beneath expansive blue ice moraines (Figure 2). RES flights 1–3 (Figure 2d) record reflectors which extend through the ice column (spanning 400–1,000 m), from the ice/bed interface, to surface sediment deposits. The detail and complexity of these reflectors are recorded by IPR. An IPR transect across Independence Hills blue ice moraine (Figure 2e) reveals numerous hyperbolic returns beneath the sediment-strewn surface, each representing point features imaged by the radar at different angles (Daniels, 2004). The steepened limbs and crests of stacked hyperbolic returns help to reveal seven linear features within the ice in Figure 2e.

Airborne RES transects also reveal steeply dipping englacial reflectors in the main flow of Horseshoe Glacier, along the subglacial extension of Patriot Hills (Figure 3a). In transects 4–6 englacial features extend from the ice/bed interface, toward the center of Horseshoe Valley, beneath >1.4 km of ice (~50 m below sea level; Figure 3a). Although reflectors in transects 4 and 5 are connected to the basal substrate, the dipping reflectors in transect 6 are completely surrounded by ice. In this last transect (transect 6), two distinct packages of reflectors are recorded, ~100 and 240 m away from the valley sidewall. These reflectors extend toward the center of Horseshoe Valley at a reduced inclination to those highlighted in transects 4 and 5.

Airborne RES transects 7–9 (Figure 3c), collected just outside the confines of Horseshoe Valley (Figure 1; where ice flows from Horseshoe Valley's neighboring Independence Trough, toward the Institute Ice Stream and the Filchner Ronne Ice Shelf (Winter et al., 2015)), reveal similar englacial reflectors to those recorded in RES transects 4–6 (Figure 3a). In Figure 3c inclined reflectors are recorded along the edge of a subglacial highland, where the englacial features extend up, and into the ice flow at angles of ~55° to 63° (from vertical). In transects 7 and 8, these reflectors extend from the raised basal substrate beneath buckled and disrupted englacial stratigraphic layers. Sequential radargrams show how the spatial amplitude and frequency of these englacial layers decrease down flow, until largely straight and parallel layers are recorded in transect 9, where the bed elevation is lower. In this final radargram dipping englacial reflectors are present near the ice/bed interface but they are not connected to the bed.

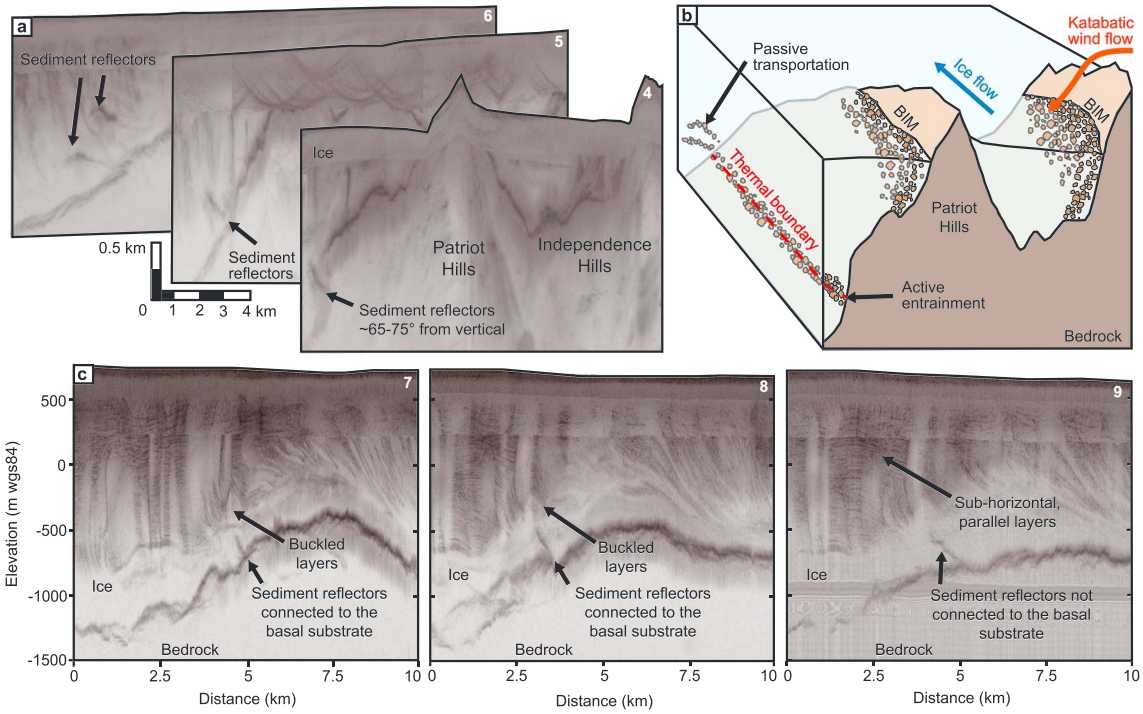

Figure 3. Englacial reflectors in Horseshoe Valley, detected more than 1.4 km below the ice sheet surface. (a) Airborne RES flights 4–6 record reflectors, thought to have derived from debris-rich ice. Reflectors extend from the subglacial mountain side to the center of Horseshoe Glacier. Note that the uppermost 200 samples (~500 m) of the ice column are poorly resolved as a function of 2-D synthetic aperture radar (SAR) processing (see section 3). (b) A schematic representation of (a), highlighting sediment entrainment along the local thermal boundary (and in compressive BIAs where katabatic winds sublimate the ice surface). When subglacial topography changes and sediments are no longer available for entrainment at the elevation of the local thermal boundary (e.g., RES transect 6), regional ice flow will passively transport glacially entrained clasts down flow, toward the local grounding line. (c) Radargrams 7–9 reveal similar englacial reflectors that extend from a subglacial highland region. We hypothesize that these reflectors evidence basal sediments entrained beneath buckled englacial layers in RES transects 7–8. When the subsurface topography changes down flow in RES line 9 these englacial sediments are detached from the basal substrate and passively transported down flow.

The steeply dipping reflectors we highlight in airborne RES transects are recorded in a variety of radargrams, which have been collected along flight paths of varying orientation. In these radargrams, reflector shape, size, and reflectivity vary with depth through the ice column, and with increasing distance down flow. We therefore interpret these reflectors as arising from sediment entrained within the basal layers of the WAIS. This hypothesis is supported by basal clasts in local blue ice moraine sequences (Figures 2b and 2c) and the occurrence of hyperbolically defined point-like features in an IPR transect (Figure 2e). We reject alternative interpretations that the reflectors could represent off-line reflectors from valley sidewalls (e.g., Holt et al., 2006) or changes in the crystal fabric of the ice (e.g., Eisen et al., 2007) because sequential ice-penetrating radargrams reveal reflectors at different depths, angles, and distances from the mountain front. These two processes also fail to account for the occurrence of subangular and subrounded clasts with millimeter-scale striations in local blue ice moraine sediments (Figures 2b and 2c).

Mie scattering analysis allows us to explore deep subsurface echoes mathematically. Analysis produces physically plausible particle sizes, in the region of 3–10 cm in RES transects 5, 6, 8, and 9, when we assume an ice/debris ratio of 90:10 (Figure 4 and supporting information), which is consistent with observed sediment concentrations in Antarctic ice cores of 0.3–3.4% (Tison et al., 1993) and 12–15% (Gow et al., 1979). These particle sizes correlate with measured grain sizes within the Patriot Hills blue ice moraine (Westoby et al., 2015). We repeat Mie scattering analysis for a range of attenuation values to account for the uncertainty in radiometric calibration and find that estimated particle sizes remain comparable with measured sediment grain sizes as long as the ice/debris ratio is equal to or greater than 90:10 (see supporting information for further description of methods and results). This analysis supports our interpretation that these deep reflectors are indicative of entrained sediments.

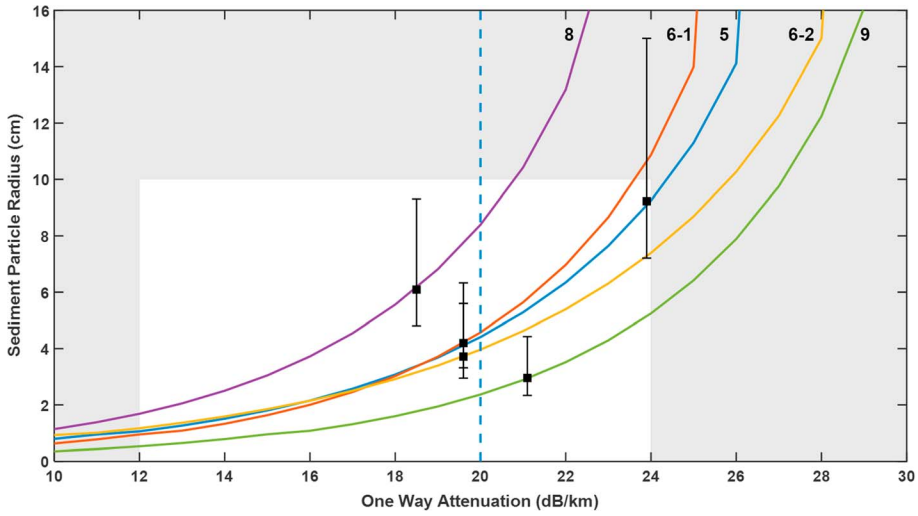

Figure 4. Sediment sizes required to produce the recorded power from deep reflectors in various airborne RES transects as a function of the englacial attenuation rate at a 10% fractional volume of sediment. The blue dashed line is the mean modeled attenuation rate (Matsuoka et al., 2012). Black squares show the optimal estimate of sediment size for each deep reflector and error bars give the variation in particle size for fractional volumes from 3 to 20%. The white rectangle highlights the range of physically plausible sediment grain sizes and attenuation rates. Even considering uncertainty in attenuation and fractional volume, the observed echo powers in transects 5, 6, 8, and 9 are consistent with scattering from entrained sediments (and observed sediment sizes in local blue ice moraine deposits).

4.2. Englacial Debris Volume

To estimate the area, volume, and mass of englacial debris in and around Horseshoe Valley, polygons are used to define the extent of debris reflector bands within zones of off-line reflectors and hyperbolic radar returns in the nine airborne RES transects we examine. Approximate area calculations are provided in Table 1. To convert area to volume, known distances between RES flight lines were fed into equation 1, which denotes a standard equation, developed to calculate the volume of a frustum (V_f) from two given areas (A_1, A_2).

$$V_f = (\text{distance between transects}/3)\times\left(A_1 + A_2 + \sqrt{(A_1 \times A_2)}\right) \quad (1)$$

This calculation yields estimates of ~506×10^6 m^3 of debris-rich ice between airborne RES transects (which cover <10% of Horseshoe Valley Glacier). Assuming a standard high limestone density of 2,560 kg/m^3

Table 1
Approximate Debris Calculations From Sediment Reflectors in Nine Airborne RES Transects

RES flight number	Area ($\times 10^3$ m^2)	Distance between RES transects (m)	Debris volume ($\times 10^6$ m^3)	Mass 100% ($\times 10^9$ kg)	Mass 10% ($\times 10^9$ kg)	Mass 20% ($\times 10^9$ kg)
1	92	-	-	-	-	-
2	55	1,690	123	315	32	62
3	21	1,596	59	150	15	30
4	8	-	-	-	-	-
5	8	3,426	27	70	7	14
6 (reflector 1)	15	12,611	143	365	37	74
6 (reflector 2)	26	6,000[a]	97	248	25	50
7	23	-	-	-	-	-
8	30	1,104	29	75	7	14
9	12	1,396	28	73	7	14
Total:	290×10^3 m^2		506×10^6 m^3	1296×10^9 kg	130×10^9 kg	258×10^9 kg

Note. Mass of debris = total volume of debris × 2,560 (representing the density of limestone in kg/m^3 (Ingham, 2010)). Mass 100% assumes 100% debris block. Mass 10% approximates 90% ice and 10% debris, etc.
[a]Estimated distance due to lack of 3-D data.

(Ingham, 2010), which reflects regional lithology (Sugden et al., 2017), these approximations suggest conservative estimates of >130 million metric tonnes of englacial sediment in and around Horseshoe Valley (using an ice/debris ratio of 90:10). In context, this estimate equates to a sediment yield of ~75 kg/m^2 were this mass to be distributed across the surface of Horseshoe Glacier.

5. Discussion

Basal thermal regimes control subsurface erosion, meltwater production, basal slip, and sediment entrainment in glacial systems (Boulton, 1972; Weertman, 1961, 1966). In areas where bed topography favors convergent ice flow, ice velocities will increase and produce more heat by internal deformation and/or basal sliding (Sugden, 1978). These two fundamental concepts govern sediment entrainment and sediment transport in large ice sheets.

5.1. Sediment Entrainment and Transfer in Blue Ice Areas

We propose that basal sediments in Horseshoe Valley are entrained within glacial ice through repeated melting and freezing processes at the glacial bed, characteristic of warm-based ice (Alley et al., 1997; Hubbard & Sharp, 1993). When clasts are englacially entrained along the margins of Horseshoe Valley, ice flow will transfer these sediments upward, with ice flow, toward blue ice surfaces. On the leeward side of Independence Hills, this flow trajectory is evidenced by stacked hyperbolic reflectors and sheets of englacial sediments. We hypothesize that these reflectors represent planes of concentrated sediment in the ice, formed in response to the compression imposed by ice flow toward the mountain front.

5.2. Sediment Entrainment and Transfer at Depth

Regions of freeze on and melt in Antarctica will change spatially and temporally as the local glacial thermal boundary reacts to ice flow across varied and complex topography and glacial-to-interglacial changes in ice thickness. The impact of varying relief is apparent in transects 4 and 5 (Figure 3a), where sediments are entrained through regelation processes along the subglacial extension of Patriot Hills. We hypothesize that entrainment occurs at the thermal boundary between warm- and cold-based ice. When subglacial topography changes in transect 6, and conditions for entrainment are no longer met (when the local thermal boundary is likely to be elevated with respect to the lower subglacial topography), sediments cannot be incorporated into the glacier. These processes are shown schematically in Figure 3b. This figure demonstrates sediment entrainment along the margins of Horseshoe Valley when the local thermal boundary intersects the ice/bed interface, and passive transportation of previously entrained debris-rich ice when conditions for entrainment are no longer met. During this passive phase, previously entrained sediment is "smeared out" in the direction of flow (Stokes & Clark, 2002). This down-flow attenuation eventually lowers the thickness of englacial sediment layers beyond the resolution of current radar systems, which accounts for the reduction and eventual loss of sediment derived reflectors in airborne RES transects collected further down flow, at ever-increasing distances from sediment sources.

Similar methods of entrainment and transfer are recorded in RES transects 7–9 when englacial reflectors are imaged along the side of a topographic upland (Figure 3c), situated just outside the confines of Horseshoe Valley. In these radargrams, reflectors with radar scattering indicative of sediment particles in the range of 3–10 cm (see Figure 4 and supporting information) are recorded beneath buckled englacial stratigraphic layers. These layers develop as a result of compression due to ice flow around the bedrock obstacle, which initiates and maintains a local thermal boundary between slow (colder) flow around the bedrock obstacle, and faster (warmer) ice flow above the obstacle (Boulton, 1979; Hindmarsh & Stokes, 2008; Stokes & Clark, 2002). Sediment is entrained along this interface through melting and freeze-on. Just like sediment entrainment and transfer in marginal blue ice areas, the presence of sediment particles in the flow field of the wider ice sheet show that sediment is still available for entrainment, and that sediments continue to be excavated, entrained, and transported in West Antarctica. However, as sediment entrainment and transportation processes will vary spatially and temporally as a result of subglacial topography, sediment availability, ice flow, and ice temperature, changing conditions (for example, in ice thickness) will alter sediment abundance and distribution in Antarctica, impacting Southern Ocean sediment delivery.

6. Conclusions

Steeply dipping englacial reflectors in regional airborne RES and hyperbolic reflectors in local ground-based IPR transects are evidence of debris-rich ice in the WAIS. In Horseshoe Valley katabatic winds promote and maintain extensive blue ice areas in the lee of nunataks, where basal sediments are entrained at the ice/bed interface by repeated melting and refreezing of warm-based ice. These sediments are transported through the ice column to the glacial surface by compressive ice flow, enabling basal sediment exhumation in debris bands and blue ice moraines. Glacial thermal regimes also facilitate sediment entrainment through regelation at greater depths (beneath >1.4 km of ice), at the junction between warm- and cold-based ice. Combined, these englacial sediment reflectors yield conservative estimates of 130×10^9 kg of sediment in ice flowing in and around Horseshoe Valley. Given similar glaciological settings in the Weddell Sea Sector, and elsewhere in the WAIS, these findings suggest that the ice sheet has a significant entrainment potential unappreciated previously.

Acknowledgments

Project work was funded by the UK Natural Environment Research Council (NERC) standard grants NE/I027576/1 and NE/I025840/1. Financial support for the collection of airborne radio-echo sounding data was provided by the NERC Antarctic Funding Initiative grant NE/G03071/1. R. Culberg and D. M. Schroeder were partially supported by NSF CAREER Award 1745137. Radargrams from the Institute and Möller Funding Initiative (IMAFI) are available in SEG-Y format from https://doi:10.5285/8a975b9e-f18c-4c51-9bdb-b00b82da52b8. The comments and advice of the Editor, Edward King and an anonymous referee are gratefully acknowledged. Bernd Kulessa, Robin Bell and Jonathan Kingslake also provided helpful discussions. We thank the British Antarctic Survey for field and logistics support.

References

Aglyamov, Y., Schroeder, D. M., & Vance, S. D. (2017). Bright prospects for radar detection of Europa's ocean. *Icarus*, *281*, 334–337. https://doi.org/10.1016/j.icarus.2016.08.014

Alley, R. B., Cuffey, K. M., Evenson, E. B., Strasser, J. C., Lawson, D. E., & Larson, G. J. (1997). How glaciers entrain and transport basal sediment: physical constraints. *Quaternary Science Reviews*, *16*(9), 1017–1038. https://doi.org/10.1016/S0277-3791(97)00034-6

Boulton, G. S. (1972). The role of thermal regime in glacial sedimentation. In R. J. Price, & D. E. Sugden (Eds.), *comp. Polar geomorphology. London, Institute of British Geographers*, *Institute of British Geographers. Special Publication No. 4*, (pp. 1–19).

Boulton, G. S. (1979). Processes of glacier erosion on different substrata. *Journal of Glaciology*, *23*(89), 15–38. https://doi.org/10.3198/1979JoG23-89-15-38

Daniels, D. J. (2004). *Ground penetrating radar*, (2nd ed.). London: The Institute of Engineering and Technology. https://doi.org/10.1049/PBRA015E

Death, R., Wadham, J. L., Monteiro, F., le Brocq, A. M., Tranter, M., Ridgwell, A., et al. (2014). Antarctic ice sheet fertilises the Southern Ocean. *Biogeosciences*, *11*(10), 2635–2643. https://doi.org/10.5194/bg-11-2635-2014

Doake, C. S. M. (1981). Tracing particle paths in the Antarctic Ice Sheet. *Journal of Glaciology*, *27*(97), 483–486. https://doi.org/10.3189/S0022143000011515

Eisen, O., Hamann, I., Kipfstuhl, S., Steinhage, D., & Wilhelms, F. (2007). Direct evidence for continuous radar reflector originating from changes in crystal-orientation fabric. *The Cryosphere*, *1*(1), 1–10. https://doi.org/10.5194/tc-1-1-2007

Fogwill, C. J., Hein, A. S., Bentley, M. J., & Sugden, D. E. (2012). Do blue-ice moraines in the Heritage Range show the West Antarctic ice sheet survived the last interglacial? *Palaeogeography, Palaeoclimatology, Palaeoecology*, *335-336*, 61–70. https://doi.org/10.1016/j.palaeo.2011.01.027

Fretwell, P., Pritchard, H. D., Vaughan, D. G., Bamber, J. L., Barrand, N. E., Bell, R., et al. (2013). Bedmap2: Improved ice bed, surface and thickness datasets for Antarctica. *The Cryosphere*, *7*(1), 375–393. https://doi.org/10.5194/tc-7-375-2013

Gow, A. J., Epstein, S., & Sheehy, W. (1979). On the origin of stratified debris in ice cores from the bottom of the Antarctic Ice Sheet. *Journal of Glaciology*, *23*(89), 185–192. https://doi.org/10.1017/S0022143000029828

Hawkings, J. R., Benning, L. G., Raiswell, R., Kaulich, B., Araki, T., Abyaneh, M., et al. (2018). Biolabile ferrous iron bearing nanoparticles in glacial sediments. *Earth and Planetary Science Letters*, *493*, 92–101. https://doi.org/10.1016/j.epsl.2018.04.022

Hawkings, J. R., Wadham, J. L., Tranter, M., Raiswell, R., Benning, L. G., Statham, P. J., et al. (2014). Ice sheets as a significant source of highly reactive nanoparticulate iron to the oceans. *Nature Communications*, *5*(1), 3929. https://doi.org/10.1038/ncomms4929

Hein, A. S., Woodward, J., Marrero, S. M., Dunning, S. A., Steig, E. J., Freeman, S. P. H. T., et al. (2016). Evidence for the stability of the West Antarctic Ice Sheet divide for 1.4 million years. *Nature Communications*, *7*(1). https://doi.org/10.1038/ncomms10325

Heinrich, H. (1998). Origin and consequences of cyclic ice rafting in the Northeast Atlantic Ocean During the past 130,000 years. *Quaternary Research*, *29*(2), 142–152. https://doi.org/10.1016/0033-5894(88)90057-9

Hindmarsh, R. C. A., & Stokes, C. R. (2008). Formation mechanisms for ice-stream margin Moraines. *Earth Surface Processes and Landforms*, *33*(4), 610–626. https://doi.org/10.1002/esp.1665

Holt, W., Peters, M. E., Kempf, S. D., Morse, D. L., & Blankenship, D. (2006). Echo source discrimination in single-pass airborne radar sounding data from the Dry Valleys, Antarctica: Implications for orbital sounding of Mars. *Journal of Geophysical Research*, *111*, E06S24. https://doi.org/10.1029/2005JE002525

Hubbard, B., & Sharp, M. (1993). Weertman regelation, multiple refreezing events and the isotopic evolution of the basal ice layer. *Journal of Glaciology*, *39*(132), 275–291. https://doi.org/10.3189/S002214300001594X

Ingham, J. (2010). Chapter 2: Building Stone. In *Geomaterials under the microscope*, (pp. 21–50). Manson Publishing, CRC Press.

Jeofry, H., Ross, N., Corr, H. F. J., Li, J., Gogineni, P., & Siegert, M. J. (2018). A new bed elevation model for the Weddell Sea sector of the West Antarctic Ice Sheet. *Earth System Science Data*, *10*, 1–21. https://doi.org/10.5194/essd-2017-90

King, E. C. (2011). Ice stream or not? Radio-echo sounding of the Carlson Inlet, West Antarctica. *The Cryosphere*, *5*(4), 907–916. https://doi.org/10.5194/tc-5-907-2011

Leventer, A., Domack, E., Dunbar, R., Pike, J., Brachfeld, S., Manley, P., & McClennen, C. (2006). Marine sediment record from the East Antarctic margin reveals dynamics of ice sheet recession. *GSA Today*, *16*(12), 4. https://doi.org/10.1130/GSAT01612A

Licht, K. J., & Hemming, S. R. (2017). Analysis of Antarctic glacigenic sediment provenance through geochemical and petrologic applications. *Quaternary Science Reviews*, *164*, 1–24. https://doi.org/10.1016/j.quascirev.2017.03.009

Liu, H., Jezek, K., Li, B., & Zhao, Z. (2001). Radarsat Antarctic Mapping Project Digital Elevation Model version 2. Boulder, Colorado USA: National Snow and Ice Data Center.

Matsuoka, K., MacGregor, J. A., & Pattyn, F. (2012). Predicting radar attenuation within the Antarctic ice sheet. *Earth and Planetary Science Letters*, *359-360*, 173–183. https://doi.org/10.1016/j.epsl.2012.10.018

Mätzler, C. (2002). MATLAB functions for Mie scattering and absorption. University of Bern: Institute of Applied Physics.

Nicholls, K. W., Corr, H. F. J., Makinson, K., & Pudsey, C. J. (2012). Rock debris in an Antarctic ice Shelf. *Annals of Glaciology*, *53*(60), 235–240. https://doi.org/10.3189/2012AoG60A014

Pierce, E. L., Williams, T., van de Flierdt, T., Hemming, S. R., Goldstein, S. L., & Brachfeld, S. A. (2011). Characterizing the sediment provenance of East Antarctica's weak underbelly: The Aurora and Wilkes sub-glacial basins. *Paleoceanography*, *26*, PA4217. https://doi.org/10.1029/2011PA002127

ReflexW (2012). version 6.1.1, *Sandmeier scientific software*, [available to download from http://www.sandmeier-geo.de/download.html].

Rignot, E., Mouginot, J., & Scheuchl, B. (2017). MEaSUREs InSAR-based Antarctica ice velocity map, version 2. Boulder, Colorado USA, NASA National Snow and Ice Data Center Distributed Active Archive Center. https://doi.org/10.5067/D7GK8F5J8M8R

Ross, N., Bingham, R. G., Corr, H. F. J., Ferraccioli, F., Jordan, T. A., le Brocq, A., et al. (2012). Steep reverse bed slope at the grounding line of the Weddell Sea sector in West Antarctica. *Nature Geoscience*, *5*(6), 393–396. https://doi.org/10.1038/NGEO1468

Shoenfelt, E. M., Winckler, G., Lamy, F., Anderson, R. F., & Bostick, B. C. (2018). Highly bioavailable dust-borne iron delivered to the Southern Ocean during glacial periods. *Proceedings of the National Academy of Sciences*, *115*(44), 11,180–11,185. https://doi.org/10.1073/pnas.1809755115

Stokes, C. R., & Clark, C. D. (2002). Ice stream shear margin moraines. *Earth Surface Processes and Landforms*, *27*(5), 547–558. https://doi.org/10.1002/esp.326

Sugden, D. E. (1978). Glacial erosion by the Laurentide Ice Sheet. *Journal of Glaciology*, *20*(83), 367–391. https://doi.org/10.1017/S0022143000013915

Sugden, D. E., Hein, A. S., Woodward, J., Marrero, S. M., Rodés, A., Dunning, S. A., et al. (2017). The million-year evolution of the glacial trimline in the southernmost Ellsworth Mountains, Antarctica. *Earth and Planetary Science Letters*, *469*, 42–52. https://doi.org/10.1016/j.epsl.2017.04.006

Tison, J. L., Petit, J. R., Barnola, J. M., & Mahaney, W. C. (1993). Debris entrainment at the ice-bedrock interface in sub-freezing temperature conditions (Terre adélie, Antarctica). *Journal of Glaciology*, *39*(132), 303–315. https://doi.org/10.3189/S0022143000015963

Turney, C., Fogwill, C., Van Ommen, T. D., Moy, A. D., Etheridge, D., Rubino, M., & Rivera, A. (2013). Late Pleistocene and early Holocene change in the Weddell Sea: A new climate record from the Patriot Hills, Ellsworth Mountains, West Antarctica. *Journal of Quaternary Science*, *28*(7), 697–704. https://doi.org/10.1002/jqs.2668

Ulaby, F. T., & Long, D. G. (2014). *Microwave radar and radiometric remote sensing*. Ann Arbor, MI: The University of Michigan Press. https://doi.org/10.3998/0472119356

Weertman, J. (1961). Mechanism for the formation of inner moraines found near the edge of cold ice caps and ice sheets. *Journal of Glaciology*, *3*(30), 965–978. https://doi.org/10.3189/S0022143000017378

Weertman, J. (1966). Effect of a basal water layer on the dimensions of ice sheets. *Journal of Glaciology*, *6*(44), 191–207. https://doi.org/10.3189/S0022143000019213

Welch, B. C., & Jacobel, R. W. (2005). Bedrock topography and wind erosion sites in East Antarctica: Observations from the 2002 US-ITASE traverse. *Annals of Glaciology*, *41*, 92–96. https://doi.org/10.3189/172756405781813258

Westoby, M., Dunning, S., Woodward, J., Hein, A., Marrero, S., Winter, K., & Sugden, D. (2015). Sedimentological characterization of Antarctic moraines using UAVs and structure-from-motion photogrammetry. *Journal of Glaciology*, *61*(230), 1088–1102. https://doi.org/10.3189/2015JoG15J086

Wilson, D. J., Bertram, R. A., Needham, E. F., van de Flierdt, T., Welsh, K. J., McKay, R. M., et al. (2018). Ice loss from the East Antarctic Ice Sheet during late Pleistocene interglacials. *Nature*, *561*(7723), 383–386. https://doi.org/10.1038/s41586-018-0501-8

Winter, K., Woodward, J., Dunning, S. A., Turney, C. S. M., Fogwill, C. J., Hein, A. S., et al. (2016). Assessing the continuity of the blue ice climate record at Patriot Hills, Horseshoe Valley, West Antarctica. *Geophysical Research Letters*, *43*, 2019–2026. https://doi.org/10.1002/2015GL066476

Winter, K., Woodward, J., Ross, N., Dunning, S. A., Bingham, R. G., Corr, H. F. J., & Siegert, M. J. (2015). Airborne radar evidence for tributary flow switching in Institute Ice Stream, West Antarctica: Implications for ice sheet configuration and dynamics. *Journal of Geophysical Research: Earth Surface*, *120*, 1611–1625. https://doi.org/10.1002/2015JF003518

Woodward, J., & King, E. C. (2009). Radar surveys of the Rutford Ice Stream onset zone, West Antarctica: Indications of flow (in)stability? *Annals of Glaciology*, *50*(51), 57–62. https://doi.org/10.3189/172756409789097469